Quaternary tectonic response to intensified glacial erosion in an orogenic wedge

AARON L. BERGER[1]*, SEAN P. S. GULICK[2], JAMES A. SPOTILA[1]*, PHAEDRA UPTON[3], JOHN M. JAEGER[4], JAMES B. CHAPMAN[5], LINDSAY A. WORTHINGTON[2], TERRY L. PAVLIS[5], KENNETH D. RIDGWAY[6], BRYCE A. WILLEMS[7] AND RYAN J. McALEER[1]

[1]Department of Geosciences, Virginia Tech, Blacksburg, Virginia 24061, USA
[2]Institute for Geophysics, Jackson School of Geosciences, University of Texas at Austin, J. J. Pickle Research Campus, Austin, Texas 78758, USA
[3]Department of Geological Sciences, 5790 Edward T. Bryand Global Sciences Center, University of Maine, Orono, Maine 04469, USA
[4]Department of Geological Sciences, University of Florida, Gainesville, Florida 32611, USA
[5]Department of Geological Sciences, U. Texas El Paso, El Paso, Texas 79968, USA
[6]Department of Earth and Atmospheric Sciences, Purdue University, West Lafayette, Indiana 47907, USA
[7]Department of Geology and Environmental Geosciences, Northern Illinois University, 312 Davis Hall, Normal Road, DeKalb, Illinois 60115, USA
*e-mail: alberger@vt.edu; spotila@vt.edu

Published online: 26 October 2008; doi:10.1038/ngeo334

Active orogens are thought to behave as internally deforming critical-taper wedges that are in rough long-term equilibrium with tectonic influx and erosional outflux. Spatial and temporal variations in climate are therefore hypothesized to have a significant influence on denudation, topography and deformation of orogens, thereby affecting wedge taper. However, the impact of the most severe transition in Northern Hemisphere climate during the Cenozoic era—the onset of glaciation—has hitherto not been empirically documented. Here we analyse the spatial patterns of denudation and deformation, and their temporal variations, in the heavily glaciated St Elias orogen in southern Alaska. Low-temperature thermochronometry, thermokinematic modelling and offshore seismic reflection and borehole data suggest that the global-scale intensification of glaciation in the middle Pleistocene epoch enhanced glacier growth and caused ice streams to advance to the edge of the continental shelf. This led to focused denudation across the subaerial reaches of the orogen and burial of the actively deforming wedge toe by the eroded sediment. We propose that this climatically driven mass redistribution forced a structural reorganization of the orogen to maintain critical taper. Our empirical results thus support decades of numerical model predictions of orogenesis and provide compelling field evidence for the significant impact of climate change on tectonics.

The kinematic evolution of real-world orogenic systems during Cenozoic cooling is an ideal but underused phenomenological venue for quantifying the interplay between plate tectonics and global climate[1–4]. Links between these interacting systems are commonly explored using numerical models of critical Coulomb wedges[5–9]. Within critical wedges, linked deformation and erosion maintain mean orogen surface gradients[10,11], such that orogen form is coupled to climatically influenced denudation pattern and intensity[5–7]. Within an orogen dominated by processes of fluvial erosion, an increase in erosional intensity is predicted to accelerate rock uplift and decrease orogen width and relief[8,9]. As glacial erosion can be more effective than fluvial erosion[12,13], a climate shift towards glacially dominated denudation should have an observable and profound impact on orogenesis. Numerical simulations of glaciated critical wedges predict that Cenozoic alpine glaciation should have intensified and redistributed erosion to follow patterns of ice flux, thereby reducing mean topography, contracting orogen width and forcing widespread structural reorganization[4,14]. Empirical studies have lagged behind models, however, and examples of these responses have not previously been linked to global cooling in a real-world orogen.

THE ST ELIAS OROGEN

The St Elias orogen is a product of the ongoing oblique collision of the Yakutat terrane into the North American plate since middle Miocene time[15–18]. Deformation is currently focused on the windward flank of the orogen within a thin-skinned fold-and-thrust belt that accommodates $\sim$3 cm yr^{-1} of shortening (Fig. 1)[15,17,19,20]. This thrust belt may be approximated as a critical Coulomb wedge, as it lies above a subducting slab and is composed of poorly indurated, offscraped Cenozoic sedimentary units with a tapered mean topographic profile[15]. The orogen has rugged coastal topography that receives heavy orographic precipitation of $\sim$3–6 m yr^{-1}, which decreases to $<$0.6 m yr^{-1} on the leeward flank[21,22]. Half of the orogen is currently covered by erosive, temperate glaciers that extend to sea level and can move hundreds of metres per year (Fig. 1). During late Pleistocene glacial maxima, regional ice coverage was nearly complete and many glaciers reached the shelf edge through now-submerged sea valleys (Fig. 1)[21]. The history of global cooling and regional glacial expansion is constrained by oxygen isotopes and syn-orogenic strata within the Gulf of Alaska, respectively

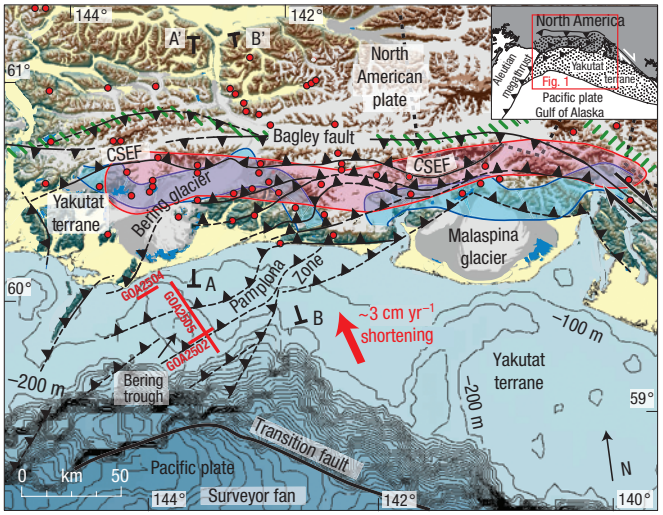

Figure 1 Thermochronometry and tectonics of the St Elias orogen. Red dots show the location of 59 AHe ages[22,32,33]. Windward flank ages range from 0.44 to 2 Myr, with the youngest ages (0.44–1 Myr) corresponding with the area shaded red. Leeward flank ages (north of the green hatched line) range from 6 to 30 Myr. The belt of most rapid exhumation (shaded red) correlates roughly with the position of the 'ELA front'[22] (shaded blue). The relief map (0–5,059 m elevation) includes offshore bathymetry (100 m contour interval), major post mid-Miocene structures[15,17,33], the modern distribution of glaciers (white) and deglaciated and ice-proximal areas covered by alluvium (yellow). The Chugach St Elias fault (CSEF) is the Yakutat–North American plate suture. Seismic profiles from Fig. 5 are shown in red.

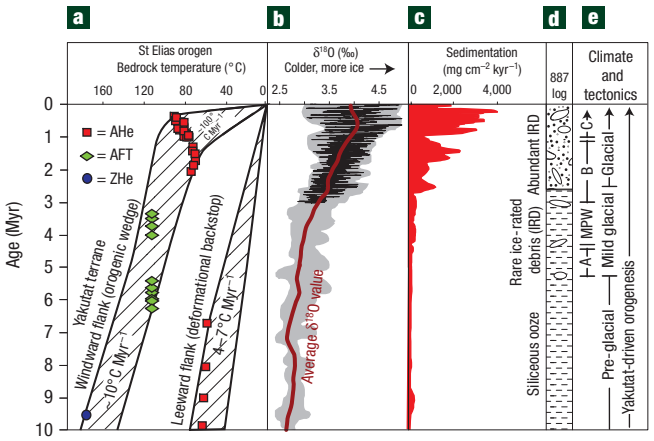

Figure 2 History of glaciation, bedrock cooling and sedimentation. a, Bedrock time–temperature paths for the St Elias orogen. Lines encompass probable cooling paths and are constrained by older AHe, AFT and ZHe ages that do not fall on the plot. **b**, Globally distributed marine records of benthic oxygen isotopes (a proxy of global ice volume and temperature) with specific values in black[26], range of values shaded and average in red[25]. **c**, History of syn-orogenic sediment accumulation in the Gulf of Alaska (mean sedimentation rate (cm kyr^{-1}) multiplied by mean sediment dry bulk density (g cm^{-3})) from Ocean Drilling Program site 887 (ref. 23). **d**, Log of sedimentary facies observed in Ocean Drilling Program site 887. **e**, Synthesis of climate events in the orogen including glacial intervals A, B and C and the mid-Pliocene warm interval (MPW).

(Fig. 2)[23–26]. Synchronous with expansion of Northern Hemisphere continental ice sheets, the concentration of ice-rafted sediments indicates that moderate glaciation was initiated by ~5.5 Myr ago (glacial interval A), but waned during the mid-Pliocene warm interval (~4.2–3.0 Myr). Glaciation returned as part of Northern Hemisphere cooling from ~3 to 2.5 Myr (glacial interval B), and, based partly on our new data, significantly intensified in the St Elias orogen in mid-Pleistocene time (deemed glacial interval C, which continues to the present). We suggest this intensification was due to a regional glacial response to a global change from 40 to 100 Kyr glacial–interglacial climate cycles, which occurred at ~0.7–1 Myr (refs 27,28). The onset of glacial intervals B and C corresponded to increases in detrital flux into the Gulf of Alaska, including a doubling of terrigenous sediment flux since ~1 Myr (Fig. 2)[23,24]. Because regional modifications of Pacific–North America plate motion are not known to have occurred in Pliocene–Pleistocene time[15,17,18,29–31], these sediment pulses suggest that glaciation increased erosion within the St Elias orogen. In particular, we contend that the onset of glacial interval C had a critical role in the evolution of the orogen.

ONSHORE LOW-TEMPERATURE BEDROCK COOLING HISTORY

Low-temperature apatite (U–Th)/He thermochronometry (AHe) constrains the exhumation pattern in the St Elias orogen[22,32,33]. Long-term, time-averaged bedrock cooling rates indicate that the most rapid exhumation since Mid-Quaternary time has been focused within a narrow east–west band on the windward flank of the orogen that correlates with the 'ELA front', or the zone between the intersection of mean orogen topography and Quaternary glacial maxima and minima equilibrium line

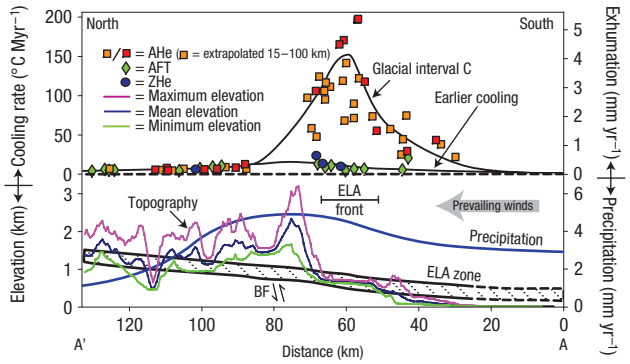

Figure 3 Variation in bedrock cooling rate, topography and climate. Cooling rates were calculated for AHe, AFT and ZHe data assuming linear cooling between respective thermochronometers. Time-averaged exhumation rates (±25%) are based on geothermal gradients accounting for thermal advection. Since the onset of glacial interval C, cooling rates have been rapid only along the windward flank of the orogen near the ELA front. Cooling rates before 3.5 Myr on the windward flank and throughout Yakutat-driven orogenesis on the leeward flank were roughly steady and considerably slower. Topography (10-km-wide swath), mean precipitation[22], the range of ELA positions[21] (modern versus glacial maxima) and the Bagley fault (BF) are shown below. Data follow transect AA', from Fig. 1.

altitudes[22] (ELA) (Figs 1 and 3). This belt of focused and rapid exhumation cuts across the structural trend of the orogen and is more concentrated than orographic precipitation, suggesting that denudation is controlled by maximum Quaternary ice flux, which should occur at mean ELA (refs 4,14,34) (Fig. 3). Exhumation is an order of magnitude slower on the leeward flank, which has

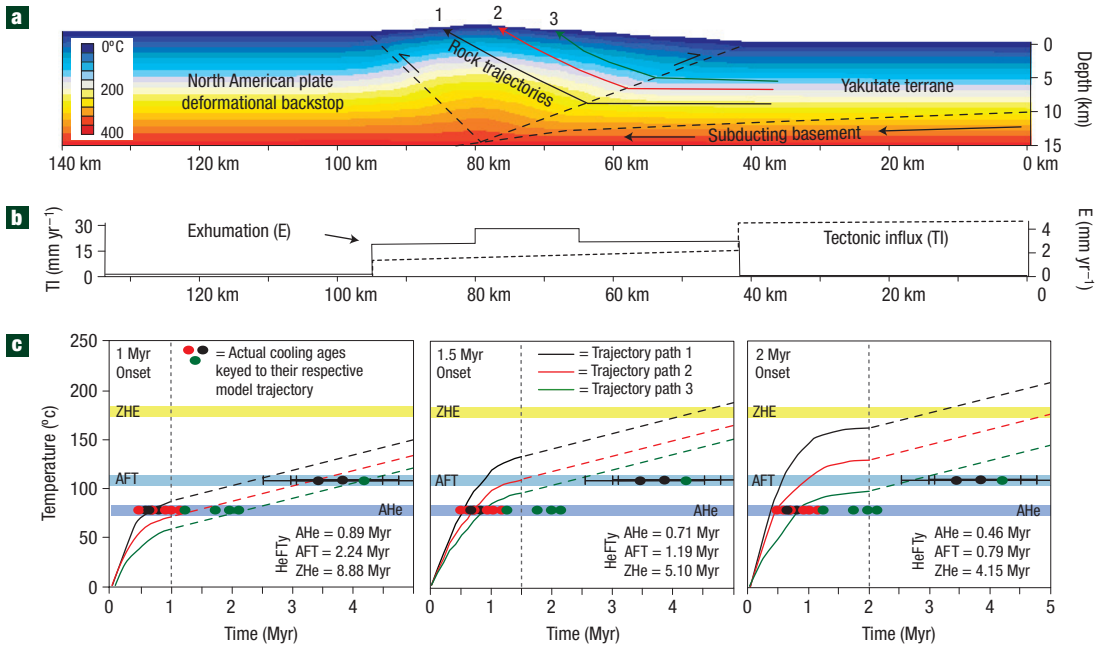

Figure 4 Two-dimensional thermokinematic model. a, Two-dimensional thermal model of the orogenic wedge after 1 Myr of accelerated exhumation, using techniques and parameters discussed in the text. **b**, Component velocity profiles for **a** at the surface. **c**, Temperature–time paths for three trajectories shown in **a**. The solid lines and dashed lines were calculated from the 2D and 1D model, respectively. Bands represent approximate closure temperatures for the AHe, AFT and ZHe mineral systems. Dots represent the actual observed ages from the Yakutat terrane colour coded for position relative to each modelled trajectory. Predicted ages calculated using HeFTy (ref. 41) are shown for trajectory path 1 on the lower right. Model parameters based on transect BB' from Fig. 1.

been interpreted to be a deformational backstop that is isolated from the deforming wedge by an active backthrust (Bagley fault) that makes the orogen doubly vergent[33] (Figs 1 and 3). Higher temperature apatite fission-track (AFT) and zircon (U–Th)/He (ZHe) thermochronometry[33,35], however, indicate that this pattern has been in place only during the past 0.5–2 Myr (Fig. 3). During this time frame, bedrock cooling rates across the windward flank of the orogen increased markedly, but have remained slow and steady on the leeward flank (Figs 2 and 3). The acceleration of bedrock cooling in the wedge is believed to have corresponded to an increase in average denudation rate from ~0.3 to 3 mm yr^{-1} (±25%), with peak erosion rates upwards of 4 mm yr^{-1} (±25%) proximal to the ELA front. To maintain critical Coulomb form, this pronounced acceleration in exhumation between the windward and leeward flanks required motion along the backthrust to increase (Fig. 3).

To further constrain the timing of accelerated erosion and the thermal evolution of the orogen, we used the finite-difference package FLAC^{3D} (Finite Lagrangian Analysis of Continua)[36,37] to solve the advective–diffusive heat equation for constrained tectonic[15,17,19,20,33], thermal[38,39] and surficial[22,33,40] boundary conditions. Details of the model are provided in Supplementary Information, Figs S1–S3, Video S1. The thermokinematic model uses rock trajectory paths based on a two-sided wedge[5,7] and an initial steady-state thermal regime developed under a uniform exhumation rate of 0.3 mm yr^{-1}. Using these parameters, the model simulates an increase to spatially variable exhumation of 3–4 mm yr^{-1} and predicts the resulting thermal histories of rock samples now exposed at the surface (Fig. 4). A one-dimensional (1D) model simulating vertical rock trajectory paths was used to constrain the pre-acceleration cooling history, owing to uncertainties in rock trajectories earlier in the history of the orogen. We ran the model three times, simulating an onset of accelerated erosion at 1, 1.5, and 2 Myr. Results indicate that erosion-induced heat advection would increase the near-surface (0–4 km depth) geothermal gradient from 25 °C km^{-1} to a maximum of 44 °C km^{-1} after 1 Myr. Thermal steady state with a near-surface geothermal gradient of 50 °C km^{-1} would only be reached after 3 Myr. Using the predicted thermal histories for each model, we calculated AHe, AFT and ZHe cooling ages using the program HeFTy (ref. 41) (Fig. 4, Supplementary Information, Note S1). Although each model run predicts AHe cooling ages that are comparable to the ages measured on the windward flank of the orogen (0.5–2.0 Myr) (refs 22,33), the 2.0 and 1.5 Myr model runs predict AFT and ZHe cooling ages that are significantly younger than observed (Fig. 4). Likewise, the cooling ages produced when the model is run to steady-state conditions are also inconsistent with the thermal history of the orogen (see Supplementary Information, Fig. S3)[42]. Only the 1.0 Myr model run results in AFT and ZHe ages that are comparable to actual measured ages (4–6 Myr and 10–13 Myr, respectively)[33,35], suggesting that the acceleration in erosion occurred in mid-Pleistocene time. The exact timing of the acceleration, however, varies in detail depending on the imposed boundary conditions and modelled rock trajectories. For example, a model with a simple vertical trajectory yields a slightly younger, although still mid-Pleistocene, constraint on the onset of accelerated onshore erosion (see Supplementary Information, Fig. S4). The mid-Pleistocene timing of accelerated denudation is therefore a robust result and is consistent with the offshore record of sediment flux (Fig. 2). These two independent temporal constraints, taken together, signify that an orogen-scale increase in erosion occurred roughly coeval with intensification of glaciation at the onset of glacial interval C.

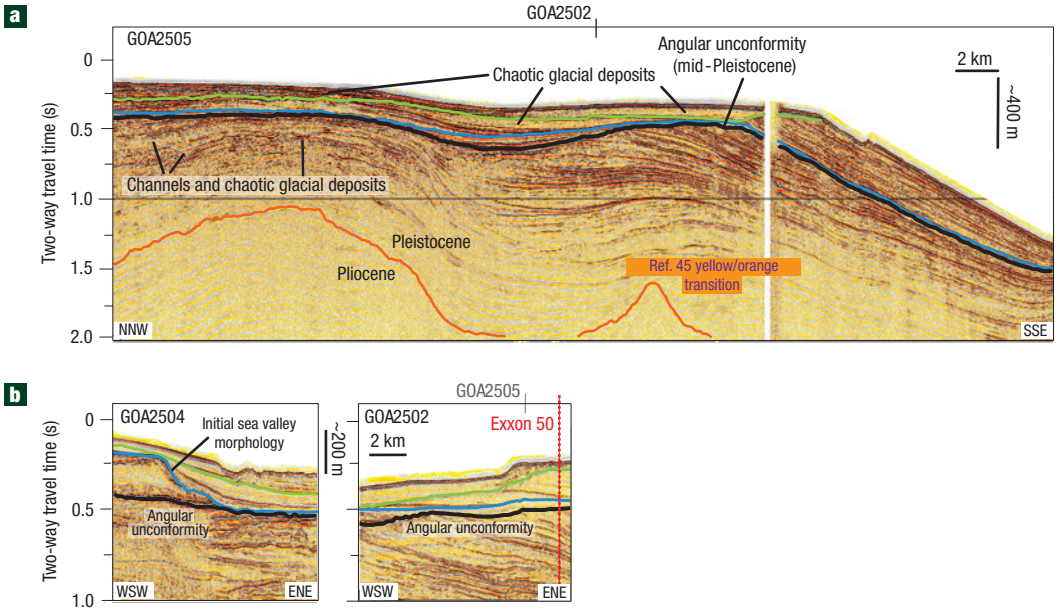

Figure 5 Seismic reflection profiles. a, Bering trough seismic profile (GOA2505). The orange line is interpreted to be the Pliocene–Pleistocene boundary based on correlation with Exxon well 50 (crossed by GOA2502) and biostratigraphy[43]. Dark coloured lines on the continental shelf represent glacial erosion surfaces and their correlative conformities. The oldest of these (black) occurred in mid-Pleistocene time and is thought to coincide with the 0.7–1 Myr middle Pleistocene transition[27,28]. Evidence of glacial erosion and deposition is limited to <25 km from the current coast below the black horizon, but is present out to the shelf edge above the black horizon. **b**, Cross-line seismic profiles GOA2504 and GOA2502 show the formation of a morphological sea valley and erosional resurfacing outside the Bering trough.

OFFSHORE RECORD OF GLACIATION AND DEFORMATION

Offshore seismic and borehole data indicate that the 1 Myr increase in denudation across the subaerial deforming wedge and the coeval increase in offshore sedimentation corresponded to an orogen-wide change in glaciation. High-resolution seismic images acquired along the Bering trough and across the seaward deformation front (the Pamplona zone) constrain sedimentation and ice coverage on the continental shelf (Fig. 5). An irregular low-angle angular unconformity occurs near the shelf edge. On the basis of correlation with biostratigraphic studies on industry wells[43] and assuming early Pleistocene sediment accumulation rates for the shelf typical of late Neogene time, this unconformity is thought to have formed during the mid-Pleistocene and marks the onset of what we refer to as glacial interval C. We interpret this unconformity to represent the first ice advance that extended beyond the present inner continental shelf (<25 km from the modern coast) and subsequently crossed the entire submarine extent of the deforming wedge to the shelf edge. Two further seismic profiles show that this unconformity occurs outside the modern sea valley and thus, was produced by a regional erosional event (Fig. 5). These profiles also show that the morphological sea valley did not form until after this regional erosional event, implying that glacial advances to the shelf edge corresponded with a transition in glacier morphology from smaller, more dispersed termini throughout the inner shelf to focused ice streams that carried greater ice discharge.

The mid-Pleistocene unconformity also represents a transition in deformation style across the submarine extent of the orogenic wedge. Before the advance of ice streams to the edge of the continental shelf, the Pamplona zone experienced long-wavelength folding and related faulting (Fig. 5). Growth strata between 1.5 and ~0.5 s indicate that these structures were buried during their latest growth, but ultimately shut-down in mid-Pleistocene time as erosion bevelled the tops of the folds. Since this shelf-wide erosional resurfacing, ~400 and ~200 m of undeformed sediment has accumulated adjacent to and in the Bering trough, respectively. Although minor shortening still occurs on the most seaward structure of the Pamplona zone outside the Bering trough[44], it is probably too small to significantly affect wedge taper. The lack of significant active shortening across the toe of the wedge is unusual, given the expectation that the frontal thrusts of a critical wedge should accommodate the greatest fraction of convergence[10,11]. These results imply that the cessation of shortening across the offshore extent of the wedge was coeval with, and causally related to, both augmented onshore denudation and lowering of the submarine critical taper by subsequent sedimentary burial. We suggest both are a product of increased glacier coverage at the onset of glacial interval C and represent examples of climate-forced tectonic change.

QUATERNARY EVOLUTION OF THE ST ELIAS OROGEN

On the basis of the above synthesis of onshore and offshore observations, we propose a kinematic model for the Quaternary evolution of the St Elias orogen and examine it in the context of change to a more intense glacial climate. Before the mid-Pleistocene glacial expansion (glacial interval C), denudation rates across the upper, subaerial portion of the orogenic wedge were relatively slow (~35 $km^2\ Myr^{-1}$ unit flux) and deformation extended from the backthrust to the offshore, forearc limit of the Pamplona zone (Fig. 6a). Since the onset of glacial interval C, however, denudation rates across the subaerial wedge have increased (~190 $km^2\ Myr^{-1}$ unit flux) and become focused at the ELA front. This change required accelerated motion along both the backthrust and a vertically stacked array of hinterland forethrusts (Fig. 6b). As the wedge contracts owing to backthrust motion, these forethrusts

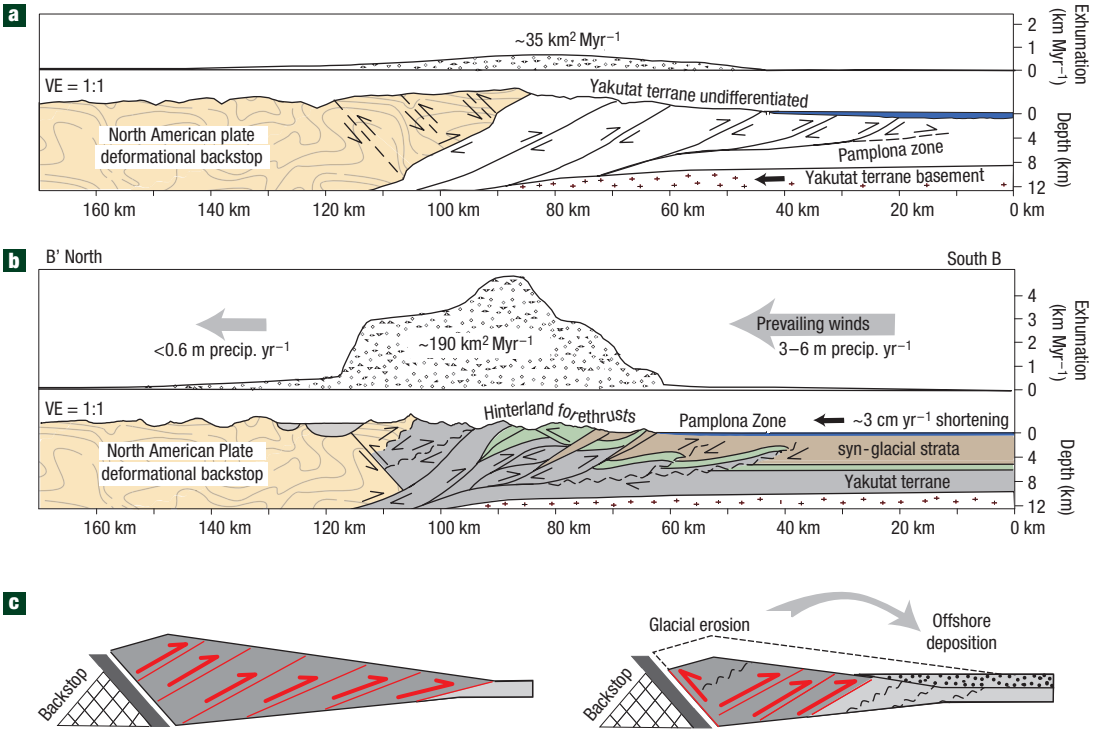

Figure 6 Proposed model of climate-related influences on orogen kinematics. a, Structural model before glacial interval C, drawn along line BB'. Exhumational flux and orogen architecture based on thermochronometry[22,33] and geologic data[15,17,33] (Fig. 1). **b**, Post glacial interval C structural model and exhumational flux. **c**, Interpretative model of the effect of glacial erosion and deposition on the orogenic wedge. Before glacial interval C (left), the wedge is wider and has greater relief. After the intensification of glaciation (right), deformation has been concentrated at the ELA front and the wedge has narrowed owing to the accumulation of shortening. Active faults are shown in red. For **a**–**c**, straight dashed lines depict structures with only minor amounts of slip and wavy dashed lines depict inactive structures. VE: vertical exaggeration.

are themselves progressively truncated and incorporated into the hanging wall of the backthrust, probably explaining the Pliocene–Pleistocene shift in deformation away from the North American–Yakutat terrane suture (Chugach St Elias fault)[33]. Coeval with these onshore changes, the offshore wedge was buried by sediment and became inactive. On the basis of mass balance, only ~20% of the sediment eroded from the subaerial wedge since 1 Myr (Fig. 6a) currently covers the inactive Bering trough segment of the offshore wedge; the remainder was probably transported farther offshore to the Surveyor fan and more distal portions of the Gulf of Alaska[23]. Periodic glacial advances may erode a fraction of this cover and redeposit it on the slope and fan, but the eroded material is replaced by renewed rapid deposition during interglacial periods[40]. This kinematic evolution fits with the classic model of critical Coulomb wedges, in which perturbations in denudation lead to structural reorganization and out-of-sequence thrusting to maintain critical taper[8–11]. In this case, Quaternary climate change seems to have focused glacial denudation across the subaerial wedge resulting in increased rock uplift through accelerated thrust motion, while coeval glaciogenic deposition lowered the submarine critical taper and stabilized offshore structures through load-induced normal stress (Fig. 6c).

A consequence of the shutting-off of the offshore Pamplona zone is that the inactive wedge has been progressively consumed by the active onshore wedge at ~3 cm yr^{-1}, such that the wedge has narrowed by ~20% since mid-Pleistocene time (Fig. 6). As long as aggressive erosion continues unabated, the St Elias orogen should continue to contract owing to the accumulation of shortening, until the inactive deformation front merges with the active deformation front and establishes a new equilibrium form. At the onset of glacial interval C, however, the zone of active deformation within the wedge narrowed by a much greater extent (~50%) (Fig. 6), suggesting that effective deformation within orogens may be confined to narrow zones within a larger wedge complex and may fluctuate depending on climatic conditions. This redistribution of deformation is consistent with model results that indicate active wedges should contract in response to an increase in fluvial erosion[8,9] or a transition to or intensification of glacial climate[4,14].

EFFECT OF GLACIATION ON OROGENESIS

The unique perspective offered by combining these distinct data sets provides an empirical view of how an orogen evolves kinematically in response to a climate shift towards intense glacial conditions. The observations imply that Quaternary deformation within the St Elias orogenic wedge has been directly influenced by glacial erosion. The trigger for the reorganization of the orogenic wedge was not the onset of Northern Hemisphere glacial conditions at ~3–2.5 Myr, but rather the intensification of glacier coverage at ~1 Myr and, perhaps, a shift in glacier morpho-dynamics towards more erosionally effective ice streams. This last process may have been in part facilitated by the formation and development of fjords and the resulting change in glacial morpho-dynamics[45]. The response of a critical wedge to climatic perturbations may

therefore function on the basis of thresholds, such that enhanced glacial erosion and glaciogenic deposition may have pushed the orogen to a tipping point, beyond which a structural reorganization and narrowing of the entire wedge were required. An implication of these results is that the onset and acceleration of alpine glaciation in late Cenozoic time should have modified denudation and deformation within numerous mountain belts worldwide, although probably on a more subtle level than the St Elias orogen, which is tectonically very active and has been subjected to one of the most extreme temperate glacial climates on Earth. This hypothesis is consistent with climate as the driver of observed changes in exhumation rates, sedimentation rates and relief within many orogenic systems over the past few million years[1,2]. Where present, glaciation may thus have a significant role in the internal processes of mountain building, empirically supporting the paradigm that orogenic architecture, kinematics and evolution may be heavily influenced by external climatic processes.

ANALYTICAL METHODS

Thermochronometry data and methods used for this work are presented in detail in supporting publications[22,33], although the primary results, the pattern and history of exhumation, are shown here (Figs 1–3). AHe, AFT and ZHe thermochronometers have typical closure temperatures of ~70, 110 and 180 °C, respectively. Closure temperatures vary in detail, depending on grain size and sample cooling rate, and were estimated using standard procedures and mineral parameters. For the background geothermal gradient in the St Elias orogen (25 °C km^{-1}), which is constrained by vitrinite reflectance data, industry wells and onshore thermochronometry[33,35,38,39], typical closure temperatures of these mineral systems reflect the history of exhumation from ~2–7 km depth[22,33]. As shown by numerical modelling results, rates of exhumation on the windward flank of the orogen are sufficiently high that advection of heat towards the Earth's surface would result in an elevated geothermal gradient. To account for heat advection, AHe-based exhumation rates from the windward flank of the orogen were calculated assuming an elevated geothermal gradient of up to 45 °C km^{-1}. The ±25% error of calculated exhumation rates is based on cumulative analytical uncertainties in laboratory measurements (±10%) and likely uncertainties in geothermal gradient.

Two-dimensional thermal profiles were calculated using the 3D finite-difference code FLAC^{3D} (ref. 36,37) in which we modified the thermal solution method to solve the advective–diffusion equation for an imposed velocity field:

$$\frac{\partial T}{\partial t} = \frac{k}{\rho C_{p(x,y,z)}}(\nabla^2 T) - \left(u\frac{\partial T}{\partial x} + v\frac{\partial T}{\partial y} + w\frac{\partial T}{\partial z}\right) - A_{(x,y,z)}$$

in which k is thermal conductivity, C_p is heat capacity, ρ is density, u, v, w is velocity in an externally fixed Cartesian reference frame and A is radioactive heat production. The model domain is 140 km long, 1 km wide and 15 km deep, representing the backstop of the North American plate and the uppermost part of the subducting Yakutat terrane (consisting of a thick sediment package overlying the subducting Yakutat terrane basement). The upper surface ranges in elevation from sea level to 2,500 m with smoothed topography. Model parameters include a fixed surface temperature of 0 °C (ref. 21). The base of the model is given a fixed temperature of 375 °C, determined from an average geothermal gradient of 25 °C km^{-1} (refs 38,39). Constrained by the architecture of the orogen[15,17,18,33], modelled rock trajectories are based on a standard two-sided wedge[5,7], which consists of conjugate thrusts along which most of the deformation is taken up. Relative motion between the North American plate and the Yakutat terrane was set at 30 mm yr^{-1} (refs 19,20), which is accommodated by the two thrust faults and by exhumation. Imposed exhumation rates are based on thermochronometry and subsidiary offshore sedimentation data[22,33,40]. The entire model domain has a thermal conductivity of 2.5 W m^{-1} K^{-1} and uniform radiogenic heat production of 0.4 μW m^{-3}.

The marine seismic data presented here were collected in 2004 aboard the R/V *Maurice Ewing*. We acquired ~1,800 km of high-resolution seismic-reflection profiles along the Gulf of Alaska continental margin using dual 45/45 cubic inch generator–injector airguns with better than 5 m vertical resolution[31]. Processing included trace regularization, normal move-out correction, bandpass filtering, muting, frequency–wavenumber filtering, stacking, water-bottom muting and finite-difference migration. Glacial erosion surfaces were identified in the data based on stratal truncations and associated chaotic reflectivity indicative of diamicton formed in ice-proximal/marginal settings[46]. Approximate chronology was established by correlating sequences beneath the angular unconformity near the shelf edge in the 2004 data with strata in nearby industry wells that were dated biostratigraphically[43] (Fig. 5). In particular, the last observation of the Pliocene planktonic foraminifera *Neogloboquadrina asanoi* at ~2,250 m below the sea floor in Exxon well 50 places the seismically imaged strata pursuant to this article in the Pleistocene and defines the angular unconformity as mid-Pleistocene.

Received 3 March 2008; accepted 19 September 2008; published 26 October 2008.

References

1. Molnar, P. & England, P. Late Cenozoic uplift of mountain ranges and global climate change: Chicken or egg? *Nature* **346**, 29–34 (1990).
2. Lamb, S. & Davis, P. Cenozoic climate change as a possible cause for rise of the Andes. *Nature* **425**, 792–797 (2003).
3. Huntington, K. W., Blythe, A. E. & Hodges, K. V. Climate change and Late Pliocene acceleration of erosion in the Himalaya. *Earth Planet. Sci. Lett.* **252**, 107–118 (2006).
4. Tomkin, J. H. & Roe, G. H. Climate and tectonic controls on glaciated critical-taper orogens. *Earth Planet. Sci.* **262**, 385–397 (2007).
5. Koons, P. O. Two-sided orogen: Collision and erosion from the sandbox to the Southern Alps, New Zealand. *Geology* **18**, 679–682 (1990).
6. Beaumont, C., Fullsack, P. & Hamilton, J. in *Thrust Tectonics* (ed. McClay, K.) 1–18 (Chapman and Hall, 1992).
7. Willett, S. D. Orogeny and orography; the effects of erosion on the structure of mountain belts. *J. Geophys. Res* **104**, 28957–28982 (1999).
8. Whipple, K. X. & Meade, B. J. Controls on the strength of coupling among climate, erosion, and deformation in two-sided, frictional orogenic wedges at steady state. *J. Geophys. Res.* **109**, F01011 (2004).
9. Stolar, D. B. *et al.* Tectonics, climate, and landscape evolution. *Geol. Soc. Am. Spec. Pap.* **398**, 241–250 (2006).
10. Davis, D., Suppe, J. & Dahlen, F. A. Mechanics of fold-and-thrust belts and accretionary wedges. *J. Geophys. Res.* **88**, 1153–1172 (1983).
11. Dahlen, F. A., Suppe, J. & Davis, D. Mechanics of fold-and-thrust belts and accretionary wedges; cohesive Coulomb theory. *J. Geophys. Res.* **89**, 10,087–10,101 (1984).
12. Brocklehurst, S. H. & Whipple, K. X. Glacial erosion and relief production in the Eastern Sierra Nevada, California. *Geomorphology* **42**, 1–24 (2002).
13. Montgomery, D. R. Valley formation by fluvial and glacial erosion. *Geology* **30**, 1047–1050 (2002).
14. Tomkin, J. H. Coupling glacial erosion and tectonics at active orogens: A numerical modeling study. *J. Geophys. Res.-Earth Surf.* **112**, F02015 (2007).
15. Plafker, G., Moore, J. C. & Winkler, G. R. in *The Geology of Alaska: Geological Society of America, Geology of North America, G-1* (eds Plafker, G. & Berg, H. C.) 389–449 (Boulder, 1994).
16. O'Sullivan, P. B. & Currie, L. D. Thermotectonic history of Mt Logan, Yukon Territory, Canada: Implications of multiple episodes of middle to late Cenozoic. *Earth Planet. Sci. Lett.* **144**, 251–261 (1996).
17. Bruhn, R. L., Pavlis, T., Plafker, G. & Serpa, L. Deformation during terrane accretion in the Saint Elias orogen, Alaska. *Geol. Soc. Am. Bull.* **116**, 771–787 (2004).
18. Pavlis, G. L., Picornell, C., Serpa, L., Bruhn, R. L. & Plafker, G. Tectonic processes during oblique collision: Insights from the St. Elias orogen, northern North American Cordillera. *Tectonics* **23**, 1–14 (2004).
19. Fletcher, H. J. & Freymueller, J. T. New constraints on the motion of the Fairweather fault. Alaska, from GPS observations. *Geophys. Res. Lett.* **30**, 1139–1142 (2003).
20. Elliott, J., Freymueller, J. T. & Larsen, C. F. Using GPS to untangle the tectonics of the Saint Elias orogen, Alaska. *Eos Trans.* (AGU 87 (52) Fall Meet. Suppl., Abstract G42A-03 2006).
21. Péwé, T. L. Quaternary geology of Alaska. *US Geol. Survey Professional Paper* **835**, 145 (1975).
22. Berger, A. L. & Spotila, J. A. Denudation and deformation in a glaciated orogenic wedge: The St. Elias Orogen, Alaska. *Geology* **36**, 523–526 (2008).
23. Rea, D. K. & Snoeckx, H. in *Proc. Ocean Drilling Program, Scientific Results: Ocean Drilling Program* (eds Rea, D. K., Basov, I. A., Scholl, D. W. & Allan, J. F.) 247–256 (College Station, 1995).
24. Lagoe, M. B. & Zellers, S. D. Depositional and microfaunal response to Pliocene climate change and tectonics in the eastern Gulf of Alaska. *Mar. Micropaleontol.* **27**, 121–140 (1996).

25. Zachos, J., Pagani, M., Sloan, L., Thomas, E. & Billups, K. Trends, rhythms, and aberrations in global climate 65 Ma to present. *Science* **292**, 686–693 (2001).
26. Lisiecki, L. E. & Raymo, M. E. A Pliocene-Pleistocene stack of 57 globally distributed benthic d18O records. *Paleoceanography* **20**, PA1003 (2005).
27. Berger, W. H. & Jansen, E. The polar oceans and their role in shaping the global environment. *AGU Geophys. Monogr.* **84**, 295–311 (1994).
28. Clark, P. U. *et al.* The middle Pleistocene transition: characteristics, mechanisms, and implications for long-term changes in atmospheric CO_2. *Quat. Sci. Rev.* **25**, 3150–3184 (2006).
29. Cox, A. & Engebretson, D. C. Change in motion of Pacific plate at 5 Myr BP. *Nature* **313**, 472–474 (1985).
30. DeMets, C., Gordon, R. G., Argus, D. F. & Stein, S. Effect of recent revisions of geomagnetic reversal time-scale on estimate of current plate motions. *Geophys. Res. Lett.* **21**, 2191–2194 (1994).
31. Gulick, S., Lowe, L., Pavlis, T., Mayer, L. & Gardner, J. Geophysical insights into the Transition fault debate: Propagating strike-slip in response to stalling Yakutat block subduction in the Gulf of Alaska. *Geology* **35**, 763–766 (2007).
32. Spotila, J. A., Buscher, J. T., Meigs, A. J. & Reiners, P. W. Long-term glacial erosion of active mountain belts: Example of the Chugach-St. Elias Range, Alaska. *Geology* **32**, 501–504 (2004).
33. Berger, A. L. *et al.* Architecture, kinematics, and exhumation of a convergent orogenic wedge: A thermochronological investigation of tectonic-climatic interactions within the central St. Elias Orogen, Alaska. *Earth Planet. Sci. Lett.* **270**, 13–24 (2008).
34. Andrews, J. T. Glacier power, mass balances, velocities, and erosion potential. *Z. Geomorphol. N.F. Suppl. Bd.* **13**, 1–17 (1972).
35. Johnston, S. A. *Geologic Structure and Exhumation Accompanying Yakutat Terrane Collision, Southern Alaska*. M.S. thesis, Oregon State Univ. (2005).
36. Cundall, P. A. & Board, M. in *Numerical Methods in Geomechanics* (ed. Swoboda, G.) 2101–2108 (Balkema, 1989).
37. ITASCA, FLAC3D (Fast Lagrangian Analysis of Continua in 3 Dimensions, version 3.1), Minneapolis (2006).
38. Johnsson, M. J., Pawlewicz, M. J., Harris, A. G. & Valin, Z. C. Vitrinite reflectance and conodont color alteration index data from Alaska: Data to accompany the thermal maturity map of Alaska. *US Geol. Surv. Open-File Report* 92–409 (1992).
39. Johnsson, M. J. & Howell, D. G. Thermal maturity of sedimentary basins in Alaska: an overview. *US Geol. Surv. Report B* **2142**, 1–9 (1996).
40. Sheaf, M. A., Serpa, L. & Pavlis, T. L. Exhumation rates in the St. Elias Mountains, Alaska. *Tectonophysics* **367**, 1–11 (2003).
41. Ketcham, R. A. Forward and inverse modeling of low-temperature thermochronometry data. *Rev. Mineral. Geochem.* **58**, 275–314 (2005).
42. Moore, M. A. & England, P. C. On the inference of denudation rates from cooling ages of minerals. *Earth Planet. Sci. Lett.* **185**, 265–284 (2001).
43. Zellers, S. Foraminiferal sequence biostratigraphy and seismic stratigraphy of a tectonically active margin; the Yakataga formation, northeastern Gulf of Alaska. *Mar. Micropaleontol.* **26**, 255–271 (1995).
44. Worthington, L., Gulick, S. & Pavlis, T. Identifying active structures in the Kayak and Pamplona Zones: Implications for offshore tectonics of the Yakutat microplate, Gulf of Alaska. *AGU Monograph* (in the press).
45. Kessler, M. A., Anderson, R. S. & Briner, J. P. Fjord insertion into continental margins driven by topographic steering of ice. *Nature Geosci.* **1**, 365–369 (2008).
46. Powell, R. D. & Cooper, J. M. A glacial sequence stratigraphic model for temperate, glaciated continental shelves, in glacier-influenced sedimentation on high-latitude continental margins. *Geol. Soc. Lond. Spec. Publ.* **203**, 215–244 (2002).

Supplementary Information accompanies the paper at www.nature.com/naturegeoscience.

Acknowledgements

We thank collaborators in studying the St Elias orogen and other colleagues for many helpful discussions and ideas, including E. Berger, R. Law, J. Buscher and particularly all STEEP (St. Elias Erosion-Tectonics Project) participants. Reviews by S. Brocklehurst and E. Kirby contributed significantly to the manuscript. Support was provided by the National Science Foundation (NSF-EAR 0409224, NSF-EAR 0408584, NSF-EAR 0735402, NSF-ODP 0351620).

Author contributions

All authors contributed to the interpretations and hypotheses presented. Writing was done by A.L.B., with contributions by J.A.S. and S.P.S.G. Low-temperature thermochronometry was carried out by A.L.B. and J.A.S. ArcGIS analyses were carried out by A.L.B. Thermokinematic modelling was carried out by P.U., with contributions by A.L.B. HeFTy age calculations were done by A.L.B. Figures were created by A.L.B (Figs 1–3 and 6), S.P.S.G. (Fig. 5) and P.U. (Fig. 4). Structural analysis and models were done by A.L.B., J.B.C. and T.L.P. Seismic reflection gathering, processing and interpretation were carried out by S.P.S.G., L.A.W., J.M.J. and B.A.W. Project planning was done by T.L.P., J.A.S. and S.P.S.G.

Author information

Reprints and permissions information is available online at http://npg.nature.com/reprintsandpermissions. Correspondence and requests for materials should be addressed to A.L.B. or J.A.S.